SIMP: SIngle Microwave Photon detection

D. Alesini, D. Babusci, M. Beretta, B. Buonomo, F. Chiarello (CNR-IFN), D. Di Bari(Tecn.), A. D'Elia (AR), L. Foggetta, G. Felici, A. Gallo, D. Di Gioacchino, C. Gatti (Resp. Naz.), C. Ligi (Resp. Loc.), G. Maccarrone, F. Mattioli (CNR-IFN), G. Papalino(Tecn.), L. Piersanti, G. Pileggi (Tecn.), A. Rettaroli (Dott.), G. Torrioli (CNR-IFN), S. Tocci (AR)

1 Introduction

The aim of the SIMP project is to develop single microwave photon counters based on current-biased Josephson junctions (CBJJ) and nanowire TES to be used as photon detector in axion searches. At LNF we focused on the CBJJ device. The absorption of a microwave photon triggers the transition of the junction to the normal state, due to an escape of the phase variable from an atom-like potential well, causing a sudden variation of the voltage across the junction. We verified on simulations that a lossless junction switches when hit by a single photon with low dark count rate, at the milliHertz level [1)]. We discuss in the following the characterization of the first and simplest prototype of photon detector, a transmission line (TL) terminated with a single JJ. The response of the junction to microwaves is investigated, to mimic the arrival of a photon while the junction is biased. This is done both by applying a continuous and pulsed rf signals. At this stage we don't expect single-photon sensitivity since the junction is galvanically connected to the transmission line acting as a dissipative system. Ultimate sensitivity will be reached by properly matching the junction to the transmission line through appropriate circuits. However, we directly proved the sensitivity of the CBJJ to an rf pulse composed of 1000 microwave photons of about 10 GHz frequency, corresponding to an energy of about 5 zJ and extrapolated this value to an estimated sensitivity to about 20-50 photons and to an energy of few hundreds of yJ.

2 Experimental setup

We tested an $Al/AlO_x/Al$ in a Leiden Cryogenics CF-CS110-1000 dilution refrigerator with a base temperature of 10 mK (figure 1). The Josephson junctions were fabricated at IFN-CNR with shadow mask evaporation with electron-beam lithography. The resist used is a copolymer/PMMA bilayer (with thickness of about 1 μm for each layer) over a Si substrate. The Al evaporation angles are 155° and 90° (thickness of about 30 nm), with an intermediate oxidation of 5 min at 3 mbar (expected thickness between 1 and 1.5 nm). The resulting junction has an area of 8 μm^2 and expected critical current and capacity of $I_0 \simeq 3$ μA and $C \simeq 1$ pF. The choice to fabricate JJ with a large area is motivated by the fact that increasing the capacitance increases the quality factor $Q = \omega_p RC$ and so the relaxation time $\tau = Q/\omega_p$ the junction takes to reflect photons back into the TL. The 5.44 mm-long Al transmission line feeding the junction is fabricated at the same time and with the same technique as the JJ, and is galvanically connected to the junction. The losses due to connection mismatches from the TL to the cryostat rf lines are minimized by keeping the impedance to 50 Ω. To achieve a 50 Ω impedance in the TL, the width of the central conductor and the distance between the latter and the grounding are linearly reduced from millimeters to micrometers. In particular, the final sizes are 10 μm for the central conductor and 5.8 μm for the gaps between the latter and the grounding. The connectors are of the SMA type with a 50 Ω impedance, as by specifications, and the cryostat is provided with 50 Ω rf lines. The only

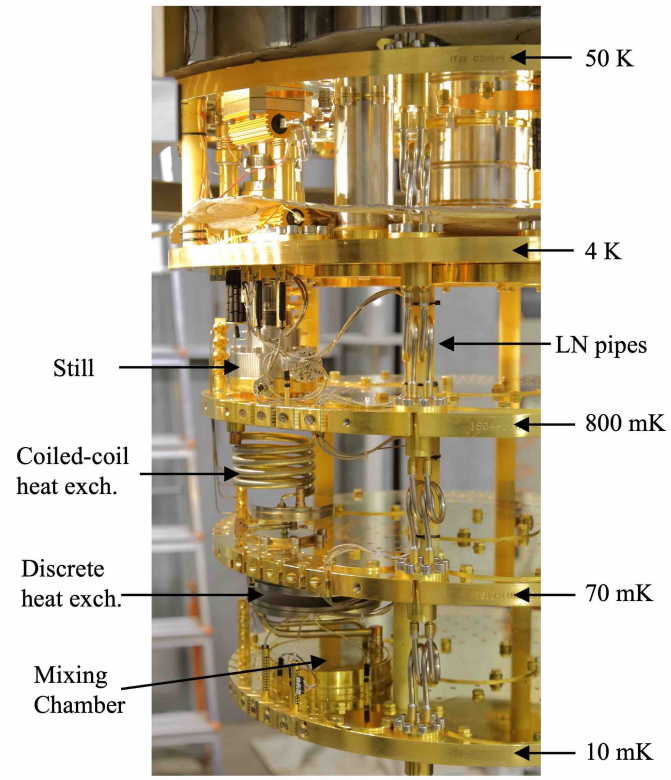

Figure 1: Detail of the Leiden Cryogenics CF-CS110-1000 dilution refrigerator, showing the plate temperatures of all the thermalization stages. The main parts where the dilution process happens are also indicated: the mixing chamber, the still and the continuous and discrete heat exchangers. LN refers to liquid Nitrogen.

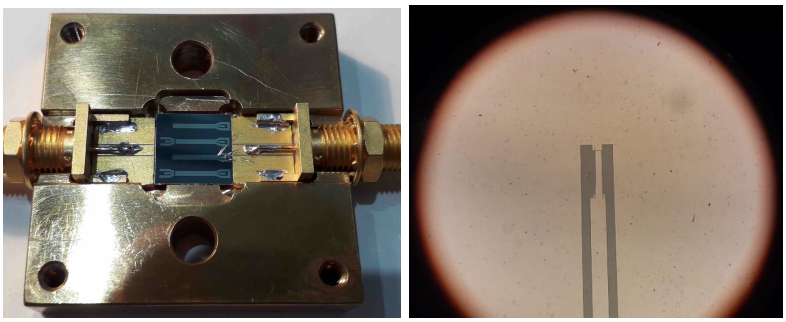

Figure 2: *Left)* Picture of the sample holder containing the chip on which the junction coupled to the transmission line is deposited. *Right)* Microscope image of the Josephson junction.

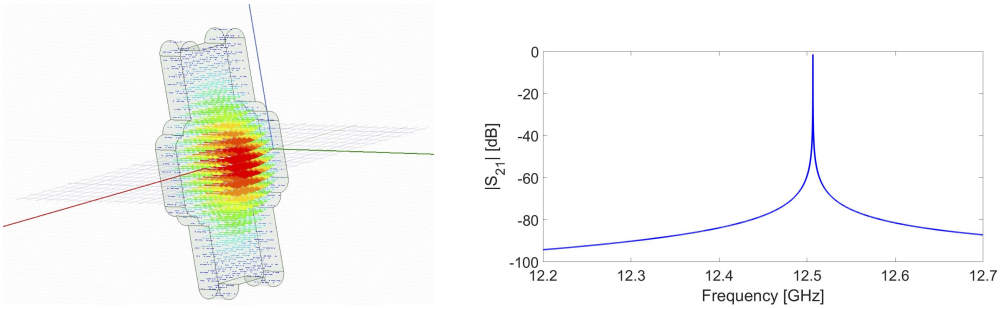

Figure 3: *Left)* Electric field lines from the simulation of the TM mode of the sample holder. *Right)* Its resonance peak at 12.51 GHz, plotted as an S_{21} scattering parameter.

uncertainty is left to the bonding wires from the chip to the TL, but because of their short lenght we expect a small effect, widely contained within the calibration uncertainty. The left picture of Fig. 2 shows the chip on which the junction and the transmission line are deposited, and is mounted in the sample holder. The tested junction is the second from the bottom of the chip with the thin wires soldered to the transmission line. The image on the right of Fig. 2 is a picture of the junction taken at the microscope.

Since the empty volume in the sample holder behaves as a resonant cavity, we simulated its geometry with ANSYS HFSS to identify its modes and avoid confusing it with the JJ resonant mode. We found a single TM mode at a frequency of about 12.51 GHz; Fig. 3 shows on the right the electric field component, which is present in all the "cavity" volume, while on the left the simulated S_{21} resonance is plotted.

The rf diagram that schematizes the measurements setup is shown in Fig. 4. The two instruments providing rf signals are in the top left of the picture, the signal generator Rohde&Schwarz SMA100B serving as a pump and the VNA Agilent E5071C. Their outputs (port 1 for the VNA) are coupled through a directional coupler (bandwidth $2 \div 18$ GHz) and directed into the same rf line going down in the cryostat, with the VNA signal passing in the "coupled" port of the directional coupler, being attenuated of 10 dB. The different temperature stages of the dilution refrigerator are shown with the dashed lines. The input rf line is interrupted with a 30 dB power attenuator at 600 mK and with another 30 dB attenuator at 10 mK, to reduce the thermal power coming from the hottest plates and environments and to avoid an overload of the JJ. Before reaching the junction, the input line encounters a double-junction cryogenic circulator (bandwidth $8 \div 12$ GHz), for

which its four ports are numbered in the picture. The fourth port is terminated with a 50 Ω load. The first part of the circulator (ports 4 and 1) avoids reflected power from the JJ to return back on the input line, while the second part (ports 2 and 3) avoids that the junction is contaminated with noise power coming from the output line, which is damped on the 50 Ω load. The microwave signals reach the single port of the JJ through a bias tee (indicated as BT in Fig. 4), which allows to simultaneously feed the junction with rf and dc. Finally, the reflected power from the JJ is directed up to the output line; we use a fifth custom rf line for this purpose. Here, the HEMT at the 4 K stage and the FET at room temperature give a total amplification of 60 dB. Then, the splitter ("Spl." in the figure) equally divides the output power: one half is sent to the second port of the VNA for S_{21} measurements and one half to the Signal Hound SM200B spectrum analyzer for power spectrum measurements. Additionally, dc wires are present to bring the current bias to the junction. The positive pole enters in the inductive port of the bias tee and then feeds the junction, while the negative pole is connected to the bias tee grounding. To avoid rf contamination on the dc lines, emi filters are used; in particular LC filters at 300 K with 1 MHz bandwidth, RCR filters at 4 K and metal powder filters at 10 mK. To screen the Josephson junction from the Earth's magnetic field, it is placed inside a lead can, as can be seen in Fig. 5.

IV characterization

We measured the characteristics I-V-curve with low frequency signals fed to the junction through the dc lines of diagram 4. These are coupled to the junction through the inductive port of the bias tee. The current-voltage room-temperature electronics scheme is very similar to that of Fig. 6. We send a voltage signal with a Keysight 33500B waveform generator on a bias resistance $R = 99.5\ k\Omega$, the current sent and the voltage read are both amplified by low-noise Stanford SR560 preamplifiers ($4\ \mathrm{nV}/\sqrt{Hz}$) and acquired by a NI USB 6366 acquisition board. The I-V characteristic shown in Fig. 7 is obtained by sending a saw-tooth waveform with repetition rate 0.117 Hz and applying 3 kHz low-pass filters to the amplifiers to reduce electrical noise. From this, the normal resistance, the voltage gap and an estimate of the critical current are obtained, being respectively $R_N = 105\ \Omega$, $V_{gap} = 380\ \mu V$ and $I_c \simeq 3.0\ \mu A$. The values are compatible with the Ambegaokar-Baratoff formula giving the expected critical current at zero temperature, $I_0(0) = (\pi/4)V_{gap}/R_N$.

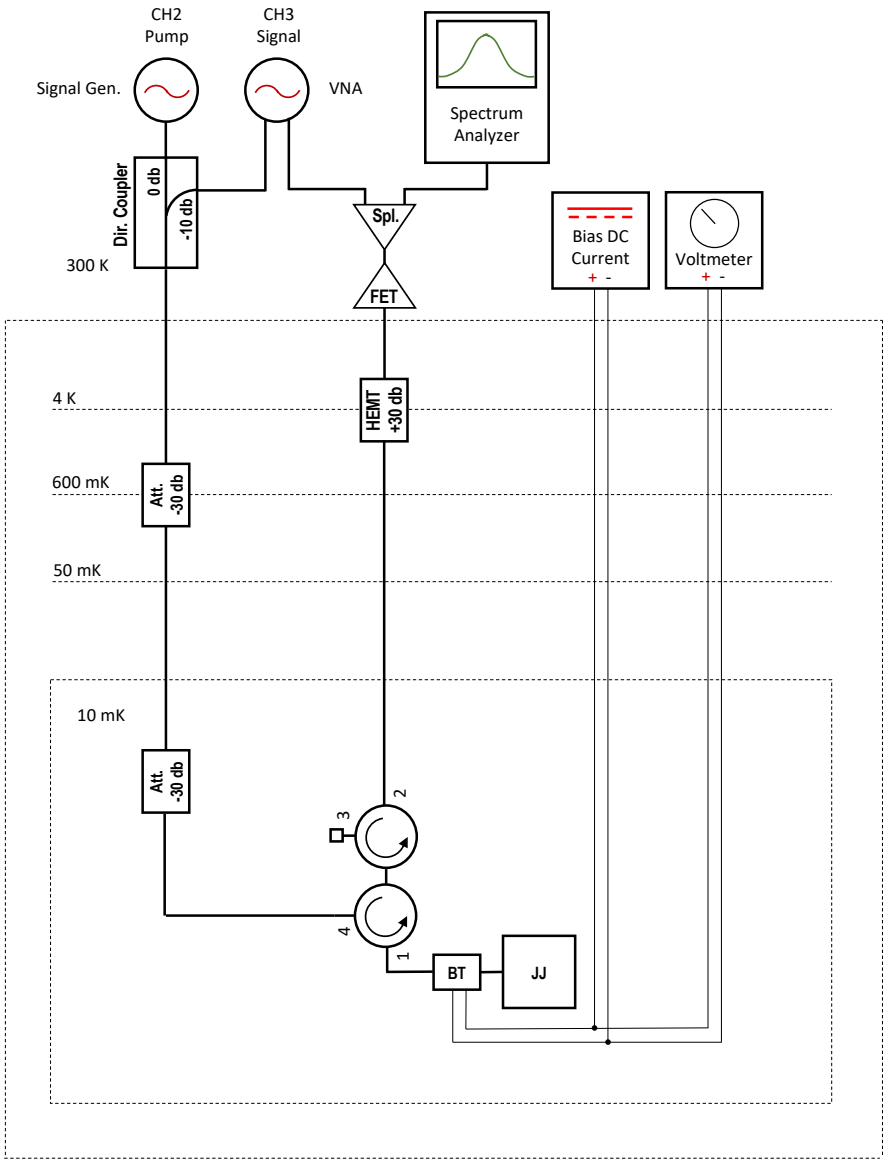

Figure 4: Schematic diagram of the rf wiring for the junction characterization. All attenuations and gains are indicated in dB units. Dc lines are also included in the picture. Refer to the text for a detailed description.

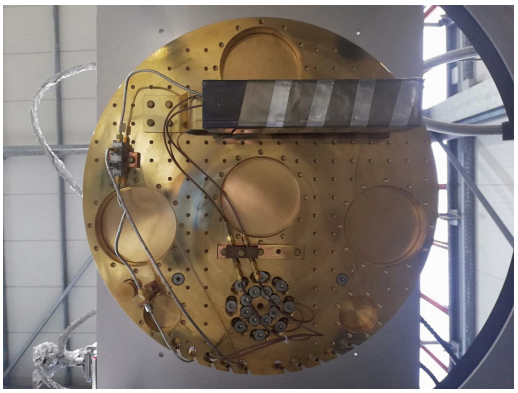

Figure 5: Bottom view of the 10 mK plate of the dilution refrigerator, where the sample is placed. The JJ is housed inside the Pb screen at the top of the picture. On the left, the double circulator is also visible, while at the center there are the metal powder filters for the dc lines.

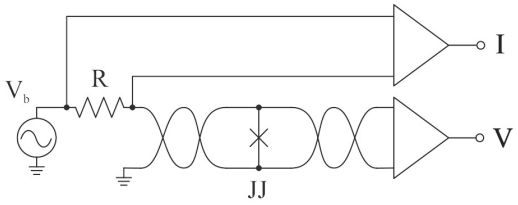

Figure 6: Scheme of the experimental setup for I-V measurement.

3 The Josephson parametric amplifier

A Josephson junction terminating a TL can operate as a four-wave mixing parametric amplifier where the amplification is provided through the Kerr term. As a starting point, we searched for the JPA resonance with a VNA frequency sweep, at different pump frequencies and power values. We found a resonance at frequency 12.1031 GHz with a power -89 dBm at the junction input as shown in Fig. 8 (red). As a reference, in the left plot we show the S_{21} profile with pump off (orange data). Then, the difference between the pump-on and pump-off data has been performed, as reported in Fig. 8 (right). From the resonance peak, the relative gain with the aforementioned stimulus conditions results in about 20 dB, while the linewidth (evaluated at -3 dB from the maximum) is about 10 MHz, giving the amplification bandwidth.

We then measured the JPA gain and noise with the spectrum analyzer. The VNA was set to the continuous wave mode, with a frequency $\nu_{VNA} = 12.0932$ GHz and power $P_{VNA} = -130$ dBm, while the pump was set to $\nu_{rf} = 12.0944$ GHz. The measurements were performed again with the pump on-pump off method, at different values of pump power. An example of the output spectrum at $P_{rf} = -88.5$ dBm is given in Fig. 9: the grey data are the output spectrum while the pump is switched off, and the only peak is the signal frequency from the VNA; the black data are the spectrum with pump on, and besides the signal, the pump frequency can be seen and the idler is present at a frequency mirroring the signal peak. The background is also amplified by the JPA.

From the background of the pump-off data we measured the HEMT noise temperature, being the only active device in the output line to add noise when the JPA is switched off. The background level is taken to the immediate left of the signal and is -94.6 dBm. Taking into account

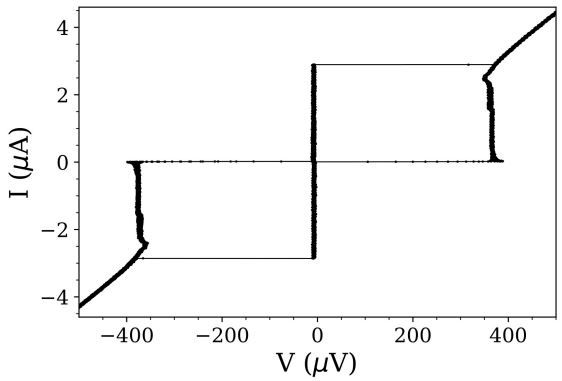

Figure 7: Measured current-voltage characteristic of the 8 μm^2 Josephson junction.

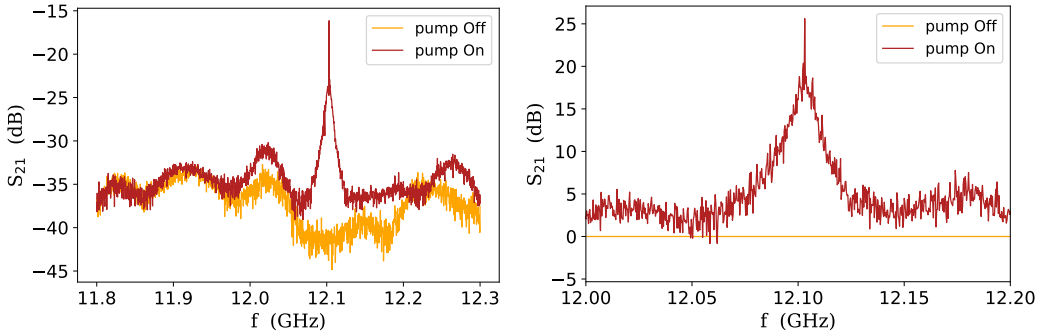

Figure 8: *Left*) S_{21} parameter from the VNA with $P_{VNA} = -115$ dBm and pump signal at $\nu_{rf} = 12.1031$ GHz and $P_{rf} = -89$ dBm (red); the data with pump off is also shown (orange). *Right*) Relative gain of the single-junction JPA, obtained subtracting the pump-on and pump-off data.

the resolution bandwidth (RBW) of the instrument set to 3×10^4 kHz, the estimated HEMT noise temperature is

$$T_n^{HEMT} \simeq 8.4\ K. \tag{1}$$

The JPA gain is obtained by measuring the signal peak absolute power with pump on and then with pump off. The result for different pump power values is shown in Fig. 10 (left): with this stimulus conditions, the maximum observed JPA gain is about 18 dB. The noise temperature is shown in Fig. 10 (right) referring the noise power to the JPA input by dividing by its gain. The minimum noise temperature is about 1.3 K. The two points above 2.5 K correspond to regions in which the background was highly amplified, giving a very bad signal-to-noise ratio. In that case the Josephson amplifier becomes unstable and behaves as an oscillator. Actually, Fig. 10(right) is the noise temperature of the JPA plus HEMT amplification chain. An estimation of the noise only due to the JPA (at the point with maximum gain and minimum noise temperature) can be done by subtracting the HEMT noise referred to the JPA input:

$$T_n^{JPA} = 1.3\ K - 8.4\ K/10^{18/10} = 1.17\ K\,. \tag{2}$$

This indicates that the amount of noise is two quanta, since the obtained temperature is twice the standard quantum limit at 12 GHz, $T_{SQL} \simeq 580\ mK$.

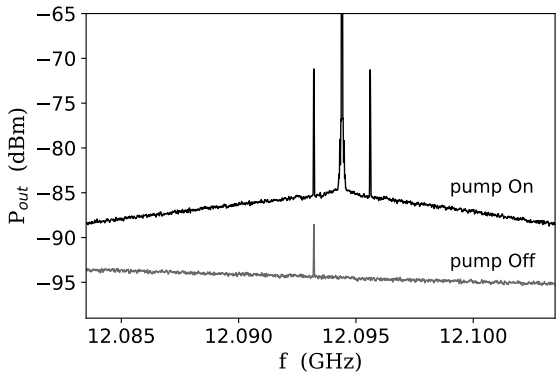

Figure 9: Pump off (grey) and pump on (black) output spectra with the signal from the VNA at a frequency $\nu_s = 12.0932$ GHz and power $P_s = -130$ dBm, and with pump frequency $\nu_{rf} = 12.0944$ GHz and power $P_{rf} = -88.5$ dBm. The peak at 12.0956 GHz is the idler frequency.

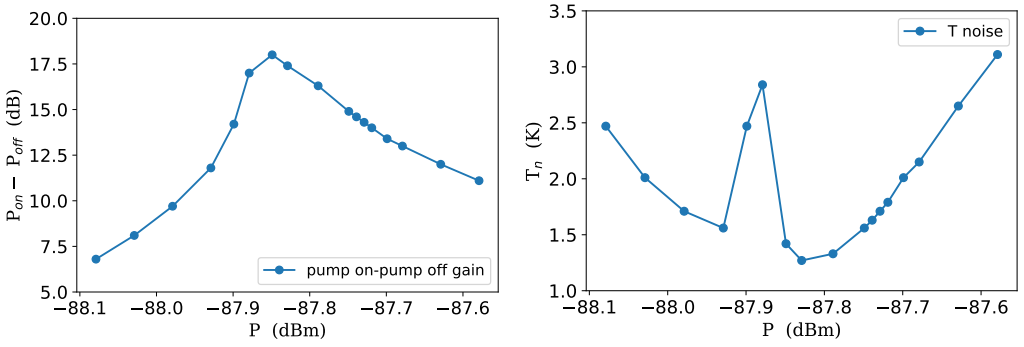

Figure 10: *Left*) Single-junction JPA gain obtained with the pump on-pump off method as a function of the pump power. *Right*) JPA noise temperature as a function of the pump power.

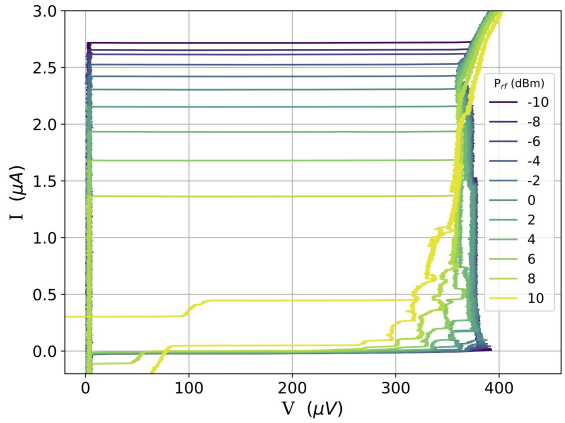

Figure 11: Current-voltage characteristics of the junction for different pump powers at a pump frequency of $\nu_{rf} = 8$ GHz. In the legend, the power values from the signal generator are reported.

4 Resonant activation

We measured the junction response in the presence of continuous and pulsed rf waves. The resonant activation, the transition of the junction from the superconductive to the normal state, is seen in IV-characteristics in the presence of microwaves and in escape measurements. The escape rates are obtained in different configurations of bias currents and rf excitations. The resonance condition is fulfilled when the frequency of incoming photons matches the proper oscillation frequency of the junction, or, in the quantum picture, when the photon energy matches the levels separation-energy. We are here in a semiclassical regime where noise temperature is greater than the crossover temperature, so that quantum escape and thermal activation processes coexist, and where the junction de-excitation time is of order $50-100$ ps so that energy levels are broadened with a large bandwidth, more than 1 GHz.

4.1 IV in presence of microwaves

The measurement setup is the same as for the low-frequency IV characterization, but now continuous radiofrequency is sent to the junction from the signal generator through the rf pump line. We expect that the presence of microwaves reduces the escape current, the current at which the JJ switches to the normal state. In fact, this is shown in Fig. 11, where the IV characteristics are plotted for increasing pump power values, at the frequency $\nu_{rf} = 8$ GHz. In this figure, the steps corresponding to the photon assisted tunneling process are also present, visible at voltage values of about V_{gap} when the bias current is returned to zero.

4.2 Escape in presence of microwaves

We measured the escape current sending continuous rf signals in the pump line while the junction is dc-biased. Microwaves are coupled to the capacitive port of the bias tee and reach the junction through the Al coplanar waveguide. The presence of microwaves facilitates the escape process, in particular when the rf frequency is in resonance with the plasma frequency of the junction. In this case, we observe escape events occurring at currents well below the critical current.

In Fig. 12 we report a density plot of the experimental switching distribution for increasing power P, measured at generator, at fixed frequency f=11.5 GHz. The dotted line for P=-20 dBm

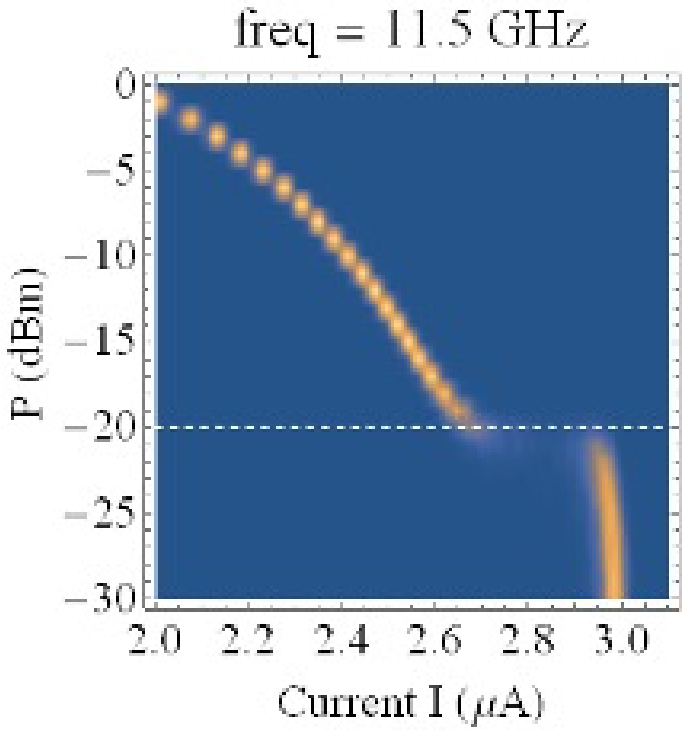

Figure 12: Density plot of the experimental switching distributions vs. variable power, for fixed microwave frequency f=11.5 GHz. Note the peak due to microwaves on the left, above the dotted line, and the thermal/quantum peak on the right, below the line.

separates the regions where transition caused by microwaves, lower currents, or thermal/quantum activation, higher currents, dominate. Here we observe the sudden variation in the switching current. The escape current distributions corresponsing to this region are shown in Fig. 13. The points in the plot are the experimental escape distributions obtained from the data of the switching currents. The different colors are related to different rf conditions, as indicated by the frequency values and power in the plot. Since the junction is sensitive to the number of photon arriving within a relaxation time τ, about 100 ps, we converted the power P_{RF} into photon number N_{ph} according to $N_{ph} = P_{RF} \times \tau/\hbar\omega$. In Fig. 13, the right peaks are related to thermal escapes, while the left peaks are due to premature switchings caused by the presence of microwaves. The resonant activation is clearly visible at different stimulus conditions. The solid curves in the plot are derived from a model describing the escape process when rf is applied to the junction. Despite the average power reaching the junction $P_{RF} = 100$ fW is rather high for a nanobolometer, it must be stressed again that this device is not sensitive to power but to the number of photons arriving within a relaxation time. In this sense, these results gives us a first indication of the sensitivity of the junction to few microwave photons.

5 Pulsed measurements

In order to test the device in a configuration as close as possible to that of a photon detector, we sent to the junction RF pulses to measure the detection efficiency. However, the minimum possible pulse-width with our RF generators is about 5 ns, much larger than the relaxation time $\tau \sim 100$ ps,

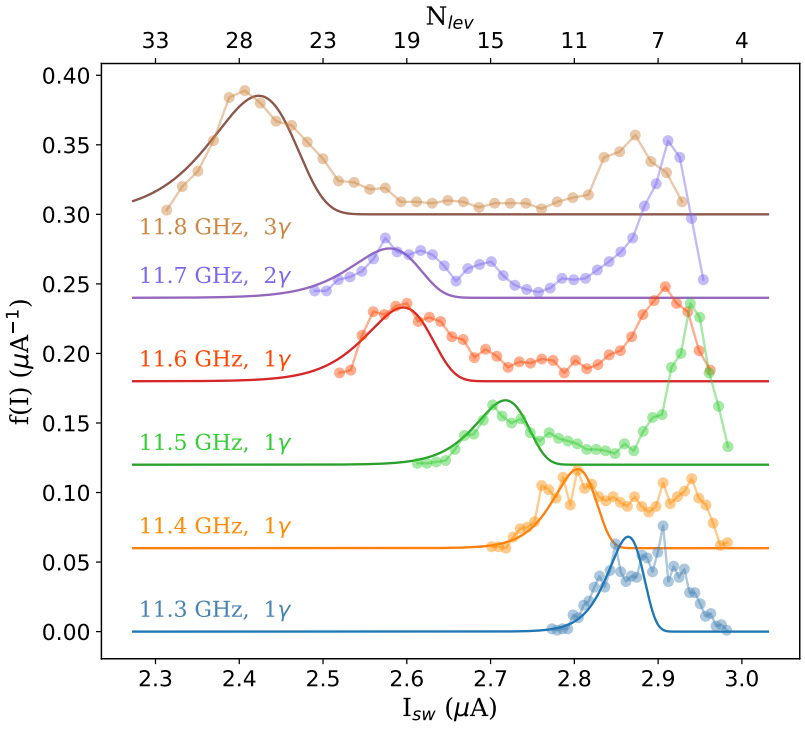

Figure 13: Escape distributions vs. bias current in the presence of microwaves. The points are experimental data, the frequency and number of photons in a relaxation time corresponding to the rf power are indicated on the left. The solid curves are the expected switching distributions in the presence of microwaves.

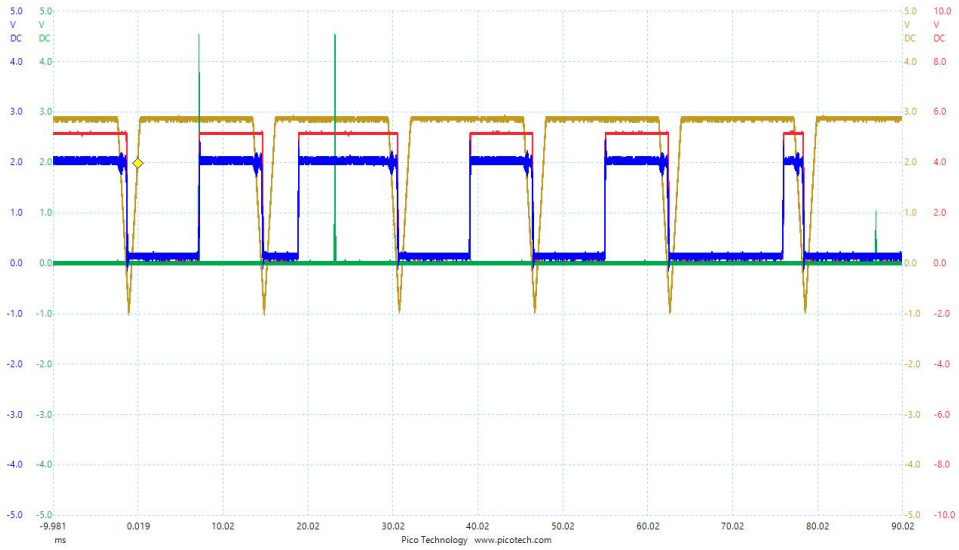

Figure 14: Signals involved in the pulsed measurements of the junction lifetime, visualized on a PicoScope digital oscilloscope. Yellow indicates the bias current arbitrary waveform, blue is the voltage across the junction, which undergoes a sudden change from zero to a finite value when the junction switches, red is the TTL signal accompanying the JJ voltage above a certain threshold, and green is the 10 ns rf pulse starting 7 ms after the current has reached its maximum value. The current ramps have repetition rate of 62.8 Hz. Note that the rf pulse is always present in all the cycles, but due to the oscilloscope slow samplings on this timescales it is not always visible on screen.

so that the sensitivity to few photons can again only deduced by extrapolation of the experimental results.

The electronics logic is very similar to the setups previously described for the escape measurements, but now the rf signal generator has to be properly triggered. The arbitrary waveform generated by the Keysight 33500B to current-bias the junction is shown in yellow in Fig. 14, which gives an oscilloscope visualization of the signals involved during lifetime measurements. The waveform consists in a first ramp until the desired bias value is reached, after which the current is maintained constant. Then, the current is ramped down to some small negative value to make the junction return to the superconducting state, and the cycle repeats. A TTL signal is generated by the Keysight 33500B at the end of the current ramp-up and triggers the signal generator Rohde&Schwarz SMA100B. The trigger is also sent to the acquisition board NI USB 6366 to start to count time. After 7 ms from the trigger, the Rohde&Schwarz sends an rf pulse modulated by a rectangular shape of the desired duration and height (green signal in Fig. 14). When the junction switches, its voltage raises (blue in the Figure) and from the voltage comparator another TTL is generated and acquired (red in the Figure); this constitutes an event.

As can be seen from the Fig. 14, the junction has three chances to switch: before the rf pulse, when the bias is sufficiently high to make the escape due to thermal or quantum fluctuations effective; during the pulse, for the effect of the applied microwaves; after the pulse, again caused by thermal or quantum fluctuations, but after some inefficiency effect occurred during the pulse application. The collected lifetime values are defined as the time interval between the first TTL and the second TTL, i.e. the time at which the junction has switched measured starting from the end of the current ramp-up. By analyzing the data we derived the detection efficiency for different

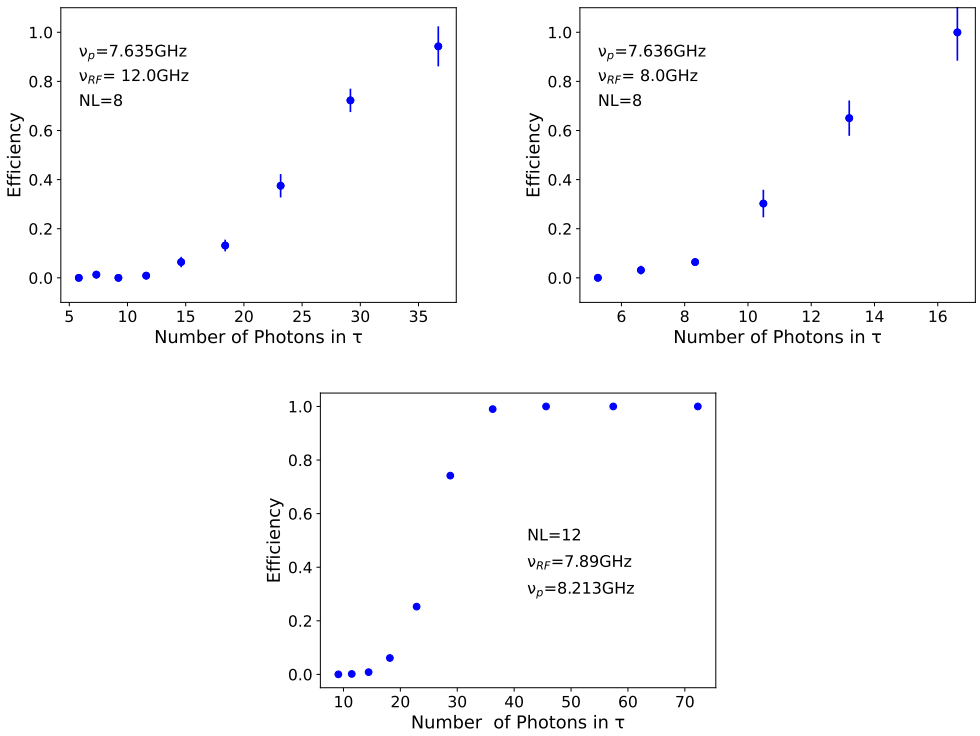

Figure 15: Efficiency as a function of the rf power, indicated as number of photons in τ (x-axis), at 12 GHz, 8 GHz and 7.89 GHz of pump frequency. The bias is slightly different in the lower graph, giving 12 energy levels instead of 8.

values of RF frequency and power and different bias currents corresponding to different height of the potential well. Few examples are shown in figure 15 where the detection efficiency of the 10 ns rf pulse is plot as a function of the incident power, again expressed as the number of photons in a relaxation time. In each picture we also indicate the estimated height of the potential well, expressed in number of levels $\Delta U = N_L \hbar \omega_p$ where ω_p is the plasma frequency of the junction. As expected, and shown by simulations, the junction switches when the number of absorbed photons (or absorbed energy) is close to the number of levels of the well (or its height).

In conclusion, we directly proved the sensitivity of a CBJJ galvanically terminating a TL to an rf pulse composed of 1000 microwave photons of 10 GHz frequency, corresponding to an energy of about 5 zJ. This measurement is limited by the minimum pulse lenght we can send with our instruments. However, simulations of the TL terminated by a JJ show that few oscillations are sufficient to induce the resonant activation of the junction, corresponsing to about 200-500 ps for 10 GHz incoming photons. This corresponds to about 20-50 photons and a sensitivity to an energy of few hundreds of yJ.

6 List of Conference Talks by LNF Authors in Year 2021

1. A. Rettaroli,"Single microwave photon counter based on current-biased Josephson junction," IEEE 14th Workshop on Low Temperature Electronics WOLTE14 (Online).

2. F. Chiarello,"Investigation of resonant activation in a Josephson junction for Axion search with microwave single photon detection," EUCAS 2021.

3. C. Gatti, "Superconducting Quantum Circuits Based on Josephson Junctions," Seminario all'interno del corso "Superconduttività Sperimentale" presso il Dipartimento di Ingegneria dell'Università Roma Tre.

4. C. Gatti, "SIMP: Single microwave Photon detection," Technologies and platforms for QT within the Q@TN Joint Lab and their application, Trento Settembre 2021.

5. F. Chiarello, "Resonant activation in Josephson junctions for Axion search:preliminary results," LSN Workshop, Laboratory of Superconducting Nanoelectronics and Center for Quantum Technologies (2021).

7 Publications

- F. Chiarello et al., "Investigation of Resonant Activation in a Josephson Junction for Axion Search With Microwave Single Photon Detection," in IEEE Transactions on Applied Superconductivity, vol. 32, no. 4, pp. 1-5, June 2022, Art no. 1100305, doi: 10.1109/TASC.2022.3148693.

- A. Rettaroli et al.,"Josephson Junctions as Single Microwave Photon Counters: Simulation and Characterization," Instruments 2021, 5(3), 25; https://doi.org/10.3390/instruments5030025.

- A. Rettaroli et al., "Single microwave photon counter based on current-biased Josephson junction," 2021 IEEE 14th Workshop on Low Temperature Electronics (WOLTE), 2021, pp. 1-4, doi: 10.1109/WOLTE49037.2021.9555446.

- C. Guarcello et al.,"Josephson-Based Scheme for the Detection of Microwave Photons," Phys. Rev. Applied 16, 054015 (2021).

- A. S. Piedjou Komnang, C. Guarcello, C. Barone, C. Gatti, S. Pagano, V. Pierro, A. Rettaroli and G. Filatrella, "Analysis of Josephson junctions switching time distributions for the detection of single microwave photons," Chaos Solitons and Fractals: the interdisciplinary journal of Nonlinear Science142, 110496 (2021) doi:10.1016/j.chaos.2020.110496.

Acknowledgement

Partially supported by EU through FET Open SUPERGALAX project, grant agreement N.863313

References

1. A. Rettaroli et al.,"Josephson Junctions as Single Microwave Photon Counters: Simulation and Characterization," Instruments 2021, 5(3), 25; https://doi.org/10.3390/instruments5030025.

2. F. Chiarello et al., "Investigation of Resonant Activation in a Josephson Junction for Axion Search With Microwave Single Photon Detection," in IEEE Transactions on Applied Superconductivity, vol. 32, no. 4, pp. 1-5, June 2022, Art no. 1100305, doi: 10.1109/TASC.2022.3148693.